Journal of Marine Science and Application (2026) 25: 1213-1224
https://doi.org/10.1007/s11804-026-00862-1

RESEARCH ARTICLE

Residual Ultimate Bending Strength of Double-Hull Oil Tankers Subjected to Combined Pitting Corrosion and Initial Imperfections

Van Tuyen Vu[1], Quang Thang Do[2], Tuan Anh Vu[1] and Huy Chinh Cu[1]

Received: 18 February 2025 / Accepted: 07 November 2025
© Harbin Engineering University and Springer-Verlag GmbH Germany, part of Springer Nature 2026

Abstract

A ship's hull inherently contains initial imperfections that develop pitting corrosion over time, particularly in steel vessels. These factors directly affect and reduce the ultimate strength capacity of the ship. This study investigates the combined effects of these damage factors on the hull girder ultimate strength of double-hull oil tankers. In addition, the study investigates the residual ultimate bending strength of double-hull oil tankers under hogging and sagging conditions through a stress distribution method incorporating several modifications. Using the selected method, different levels of initial imperfections (including slight, average, and severe levels), and corrosion volume losses (ranging from 0% to 30%) are considered to represent the damage scenario. The analysis shows that the effect of initial imperfections on the residual ultimate bending strength under extreme load was negligible (approximately 8.5% at the severe level); however, when interacting with the pitting corrosion, significant reductions of up to 37.17% and 38.50% were observed in the average cases of hogging and sagging conditions, respectively. Further evaluation of the safety factors associated with the ultimate bending moment highlights the necessity of improved structural evaluation and maintenance to ensure operational dependability and safety.

Keywords Residual ultimate bending strength; Ship structure; Initial imperfection; Pitting corrosion; Oil tanker hull

1 Introduction

The degradation of aging ship structures has been extensively studied, revealing various types of damage, including reduced thickness, imperfections, cracking, dents, and loss of structural integrity. These damages weaken the ship hull by altering its mechanical characteristics, affecting operational reliability. To expand this body of knowledge, the following section provides an overview of pertinent studies that analyzed the effects of these structural impairments on vessel hull performance.

Tekgoz et al. (2020) investigated the effects of corrosion on the strength assessment of aged and damaged ship structures. Kim et al. (2014) employed the progressive collapse analysis method using the ALPS/HULL software to evaluate the time-dependent impact of structural damage on the ultimate strength of stiffened plates. Their study examined three types of floating production storage and offloading (FPSO) vessels, incorporating the proposed corrosion model to assess the ultimate strength of the deck and outer bottom panels. A key contribution of this research was the development of a new FPSO design based on existing FPSO configurations. Yamamoto and Ikegami (1998) developed a probabilistic corrosion model based on the plate thickness measurement data. Cui et al. (2017) investigated the effects of corrosion on the ultimate strength of container ships. The study employed nonlinear finite element analysis (NFEA) to investigate the combined influence of corrosion and external loads on structural behavior. Key parameters, including initial imperfections, element sizes, boundary conditions, bending moments, and torsion, were analyzed to evaluate stress and strain distributions and to derive stress-strain relationships at the

Article Highlights

- The stress distribution method is used to determine ultimate vertical bending moments with several modifications to consider the damage factors.
- Parameters of initial imperfections and the formula used to determine corrosion loss for each structural member are presented.
- The ultimate bending moments due to single initial imperfections, pitting damage, and the combination of pitting damage and initial imperfections are collected and presented using equations, diagrams, and tables.
- The safety factors of ultimate bending moments are presented in different cases of damage.

✉ Van Tuyen Vu
tuyenvv.dt@vimaru.edu.vn

[1] Faculty of Shipbuilding, Vietnam Maritime University, Hai Phong 180000, Vietnam

[2] Department of Naval Architecture and Ocean Engineering, Nha Trang University, Nha Trang 625080, Vietnam

hull's critical state.

Paik et al. (2003) employed extensive theoretical, numerical, and experimental methods to examine the effects of uniform corrosion, pitting corrosion, fatigue cracking, and local denting damage on the structural behavior and ultimate strength of bulk carriers, oil tankers, and FPSO structures. In addition, they applied two time-dependent corrosion models to determine the thickness of aged structures and used the S-N curve approach to assess the time-dependent growth of fatigue cracks.

Vu and Yang (2017) conducted a series of studies on corrosion effects in ship structures, analyzing their impact on various ship types. Specifically, a double-hull very large crude oil carrier was used as a case study, and the incremental-iterative method (IIM), based on IACS-CSR standards, was applied to assess changes in ultimate bending moments (UBMs) and cross-sectional geometric properties, including the neutral axis position, moment of inertia, section modulus, and total cross-sectional area. Additionally, a double-hull bulk carrier (BC) and a single-hull BC were examined to evaluate the impact of three damage factors-initial imperfections, residual stresses, and general corrosion on the reductions in both the ultimate hogging bending moment (UHBM) and ultimate sagging bending moment (USBM). This analysis employed a stress distribution method at the ultimate state to determine UBMs (Vu et al., 2018).

In another study by Vu and Dong (2020), the authors assumed that general corrosion affected the deck, bottom, and side structures. IIM was applied to calculate UBMs and cross-sectional properties of the vessel. Corrosion scenarios were assumed to affect either the longitudinal members or the entire panel. The resulting reductions in UHBM and USBM, along with alterations in cross-sectional geometric properties, were documented and analyzed comprehensively. This study collectively contributes to a deeper understanding of the effects of corrosion and structural imperfections on the ultimate strength and reliability of ship hulls.

Nouri and Khedmati (2020) employed a modified stress distribution method embedded in the HULLST program to analyze the progressive collapse of corroded FPSO hull girders. They examined the effects of multiple damage-related uncertainties, including varying degrees of uniform corrosion and random pitting corrosion. These factors were analyzed to assess their influence on the UBMs, neutral axis position, and stress distribution across the structure. In a separate investigation, Piscopo and Scamardella (2021) explored the degradation of the hull girder ultimate strength (HGUS) in a 170 000 DWT BC subjected to pitting corrosion. The research employed the IIM aligned with IACS-CSR standards, together with its implementation in ANSYS Mechanical APDL, to evaluate the vessel's UBMs. Pitting corrosion was classified into nine distinct levels and assumed to manifest at various structural locations, providing comprehensive insights into its impact on hull strength.

The HGUS has been extensively analyzed in both warships and double-hull oil tankers (OTs). For warships, the acoustic-structure interaction method, combined with NFEA, was employed to evaluate the dynamic response of the hull girder under the combined effects of underwater explosions and wave-induced loads. This investigation provided detailed insights into imperfection patterns and stress distributions, with comparative analyses between experimental measurements and simulation results, demonstrating strong correlations (Zhou et al., 2021). In parallel, Putranto et al. (2022) employed an equivalent single-layer approach to assess the HGUS of OTs. Their study integrated three-dimensional finite element modeling with IIM, in accordance with IACS-CSR guidelines, to provide a robust evaluation of tanker structural performance under extreme loading conditions. From another perspective, Guedes Soares and Garbatov (1996; 1999) conducted a series of studies on the reliability of corroded OTs. Specifically, a single-hull OT was used to investigate the effects of corrosion and repair policies (Guedes Soares and Garbatov, 1996), as well as the combined impacts of corrosion, cracking, maintenance actions, and loading (Guedes Soares and Garbatov, 1999), on the reliability of ship hull structures. Kakaie et al. (2026) performed a hull girder reliability analysis for a double-hull OT. This study proposed an approach to assess the time-dependent reliability of OTs based on the HGUS.

BCs are among the most studied bulk ship types regarding corrosion stability assessment. Momčilović et al. (2023; 2024) performed an advanced study on double-hull BCs to assess the influence of pitting corrosion and uniform corrosion on the HGUS. Uniform corrosion was represented by a linear decrease in the structural thickness over time, and pitting corrosion was incorporated with two main parameters: the degree of pitting intensity (DOP) and the degree of corrosion intensity (DOC). The contribution of the different corrosion scenarios was investigated in-depth using the IIM and NFEA to provide the moment-curvature curves. A similar investigation on single-hull BCs was performed to assess HGUS via the combined influence of uniform corrosion and the stiffened components. Faqih et al. (2023) used the IIM in accordance with IACS-CSR standards to determine the UBMs, which are essential for assessing the structural behavior of corroded BCs. These investigations highlight the importance of corrosion modeling for evaluating the longevity and integrity of ship structures.

Several studies have also investigated the HGUS on OTs. Vladimir et al. (2023) analyzed a single-hull OT to calculate the HGUS and towing in waves. The study further investigated the stress contributions from towing forces and wave loads on the forecastle deck structure. The Smith

method was applied to determine the UBMs of the single-hull OT. The study included damage progression factors, such as corrosion and cracks in plating, to analyze their influence on the hull girder structural strength (Ahmadi and Ranji, 2024). In a separate study, Woloszyk et al. (2024) assessed the potential risks of structural failure related to corrosion protection design in aging OTs, using a risk-based design approach. Specifically, it was conducted on two types of large OTs: VLCCs and Handysize OTs, as corrosion damage on these vessels can have a major impact on structural safety.

Liu et al. (2018) conducted a study on a corroded container ship. In this study, the corroded hull structure was assumed to strike a rock during grounding. This scenario was used to evaluate the structural crashworthiness of the ship hull under extreme conditions. The results indicated that a 2.0 mm reduction in plate thickness due to corrosion during grounding led to a 33.8% decrease in absorbed energy.

In addition to studies on ships, Saad-Eldeen et al. (2013) selected a box girder to evaluate UBMs. This study employed two corrosion models-an average corrosion model and a realistic corrosion model to investigate their effects on the ultimate strength of the box girder structure. Numerical and experimental analyses were conducted to compare and validate the predicted decreases in UBMs.

Regarding stiffened plates exposed to pitting corrosion, previous studies have primarily focused on evaluating the structural behavior and ultimate strength of stiffened panels under axial or biaxial loading conditions (Cui et al., 2018). In assessing the influence of pitting corrosion, these studies have considered various factors, such as initial imperfections, residual stresses (Zhang et al., 2017b), panel width-to-thickness ratio, plating thickness, stiffener type and dimensions (Rahbar-Ranji et al., 2015), boundary conditions, and mesh size and type (Zhang et al., 2017b). Regarding pitting corrosion characteristics, the following parameters have been investigated: pit shape and pit depth (Feng et al., 2020; Rahbar-Ranji et al., 2015; Sultana et al., 2015; Zhang et al., 2017a, 2017b), pit location (Feng et al., 2020; Zhang et al., 2017b; Wang et al., 2023), pit diameter (Cui et al., 2018; Zhang et al., 2017a), DOP (Cui et al., 2018; Feng et al., 2020; Rahbar-Ranji et al., 2015; Zhang et al., 2017b), and volume loss (Sultana et al., 2015; Zhang et al., 2017a; 2017b).

The aforementioned studies have investigated the effect of damaging factors on ship hull structures; however, various scenarios still require further investigation. For instance, pitting corrosion has generally been modeled only on the deck, sides, and bottom structures, with volume losses (ΔV) between 0.5% and 16.0%, and is often treated as discontinuous. However, the combined effect of extensive pitting corrosion throughout the entire structure and initial imperfections remains unstudied. Therefore, this study attempts evaluate three varying levels of initial imperfections. In addition, the corrosion of pitting as a function of ΔV between 0% and 30% is investigated. Specifically, interaction between pitting corrosion and initial imperfections is highlighted as a key factor in guiding the assessment of structural performance through HGUS quantification.

In addition, this study makes a significant contribution to structural engineering because it offers important information related to the effects of common damage elements, such as initial deviations and pitting corrosion, on the load-carrying capacity of ship hull forms. These insights enable scientists to understand the impacts of such factors and provide ship owners with scientifically grounded guidance for optimizing vessel operations and maintenance management.

2 Application of methodology

2.1 Method for determining UBMs

In this study, a stress distribution assumption across the cross-section at the ultimate limit state is employed to determine the UBMs under both hogging and sagging conditions. Figure 1 illustrates this assumed stress distribution. Accordingly, the cross-sectional stresses are categorized into three zones: the yield stress zone (σ_y), the ultimate stress zone (σ_u), and the elastic stress zone. These stress values depend on the external bending moments, resulting in the hull experiencing either hogging or sagging. Based on this distribution, structural elements in the tensile zone may reach the yield stress state, whereas elements in the compressive zone may reach the ultimate stress state. Notably, structural elements aligned with the horizontal neutral axis exhibit zero stress (Paik and Mansour, 1995).

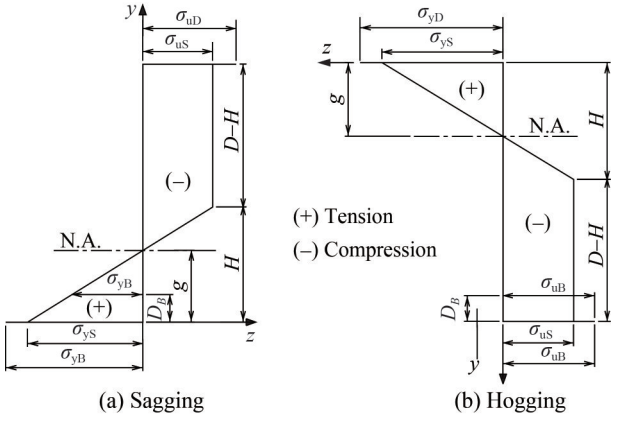


Figure 1 Assumed stress distributions at the ultimate limit state (Paik and Mansour, 1995)

The stress equilibrium is Equation (1).

$$\int \sigma_x \mathrm{d}A = 0 \tag{1}$$

where $\int \mathrm{d}A$ is the integration across the entire cross-section of the hull, and σ_x is the stress of the element.

The position of the neutral axis, g_u, at the limit state is expressed by Equation (2), as follows:

$$g_u = \frac{\sum_{i=1}^{n} |\sigma_{xi}| a_i z_i}{\sum_{i=1}^{n} |\sigma_{xi}| a_i} \tag{2}$$

where z_i is the distance from the ship's baseline (reference position) to the horizontal neutral axis of the ith structural component, σ_{xi} is the longitudinal stress of the ith structural component following the presumed stress distribution, a_i is the cross-sectional area of the ith structural component, and n is the total number of structural components, g_u is denoted as g_{us} under sagging conditions and by g_{uh} under hogging conditions.

The ultimate vertical bending moment, M_u^v, is expressed by Equation (3), as follows:

$$M_u^v = \sum_{i=1}^{n} \sigma_{xi} a_i (z_i - g_u) \tag{3}$$

where M_u^v is denoted by M_{uh}^v (positive value) under hogging conditions and by M_{us}^v (negative value) under sagging conditions. These parameters are determined by Equations (4) and (5), respectively.

$$\begin{aligned} M_{\mathrm{uh}} = {} & A_D g \sigma_{\mathrm{yD}} + A_B (D - g)\sigma_{\mathrm{uB}} + A'_B (D - g - D_B)\sigma'_{\mathrm{uB}} + \\ & \frac{A_S}{D}(D - H)(D + H - 2g)\sigma_{\mathrm{uS}} + \frac{A_S H}{3D}\left[(2H - 3g)\sigma_{\mathrm{uS}} - (H - 3g)\sigma_{\mathrm{yS}}\right] \end{aligned} \tag{4}$$

$$\begin{aligned} M_{\mathrm{us}} = {} & -A_D (D - g)\sigma_{\mathrm{uD}} - \frac{A_S}{D}(D - H)(D + H - 2g)\sigma_{\mathrm{uS}} - \\ & A_B g \sigma_{\mathrm{yB}} + \frac{A'_B}{H}(g - D_B)\left[D_B \sigma_{\mathrm{uS}} - (H - D_B)\sigma_{\mathrm{yS}}\right] - \\ & \frac{A_S H}{3D}\left[(2H - 3g)\sigma_{\mathrm{uS}} - (H - 3g)\sigma_{\mathrm{yS}}\right] \end{aligned} \tag{5}$$

where A_B, A'_{B}, A_S, and A_D are the total area of the cross-section of the bottom, inner bottom, side, and deck panel, respectively; g is the horizontal neutral axis of the cross-section; σ_{yB}, σ'_{yB}, σ_{yS}, and σ_{yD} are the yield stresses of the bottom, inner bottom, side, and deck panel, respectively; D and D_B are the hull depth and double bottom height, respectively; and σ_{uB}, σ'_{uB}, σ_{uS}, and σ_{uD} are the ultimate stresses of the bottom, inner bottom, side, and deck panel, respectively.

2.2 Method for determining the ultimate stress of structural elements

To determine the UBMs, the entire cross-section is divided into two types of structural elements: plate elements and plate-stiffener combination elements. The ultimate stresses for these elements are calculated as described below.

Plate elements (Paik et al., 2004):

For $a/b \geqslant 1$,

$$\frac{\sigma_x^U}{\sigma_{\mathrm{yp}}} = \begin{cases} -0.032\beta^4 + 0.002\beta^2 + 1.0, & \text{for } \beta \leqslant 1.5 \\ 1.274/\beta, & \text{for } 1.5 < \beta \leqslant 3.0 \\ 1.248/\beta^2 + 0.283, & \text{for } \beta > 3.0 \end{cases} \tag{6}$$

For $a/b < 1$,

$$\frac{\sigma_x^U}{\sigma_{\mathrm{yp}}} = \frac{a}{b}\frac{\sigma_{\mathrm{xu}}^*}{\sigma_{\mathrm{yp}}} + \frac{0.475}{\alpha^2}\left(1 - \frac{a}{b}\right) \tag{7}$$

$$\frac{\sigma_{\mathrm{xu}}^*}{\sigma_{\mathrm{yp}}} = \begin{cases} -0.032\alpha^4 + 0.002\alpha^2 + 1.0, & \text{for } \alpha \leqslant 1.5 \\ 1.274/\alpha, & \text{for } 1.5 < \alpha \leqslant 3.0 \\ 1.248/\alpha^2 + 0.283, & \text{for } \alpha > 3.0 \end{cases}$$

$$\beta = \frac{b}{t}\sqrt{\frac{\sigma_{\mathrm{yp}}}{E}}\,;\ \alpha = \frac{a}{t}\sqrt{\frac{\sigma_{\mathrm{yp}}}{E}}$$

where σ_x^U is the ultimate compressive stress of the plate element in the x direction, σ_{yp} is the yield stress of plating, a is the length of the plating, b is the width of plating, t is the thickness of plating, β is the plate slenderness ratio, α is the column slenderness ratio, and E is the modulus of elasticity.

Plate-stiffener combination elements (Hughes and Paik, 2010):

$$\frac{\sigma_x^U}{\sigma_{\mathrm{yeq}}} = \frac{1}{2}\left(1 + \frac{1+\eta}{\lambda_e^2}\right) - \left[\frac{1}{4}\left(1 + \frac{1+\eta}{\lambda_e^2}\right)^2 - \frac{1}{\lambda_e^2}\right]^{0.5} \tag{8}$$

where σ_{yeq} is the equivalent yield stress, λ_e is the effective column slenderness ratio, σ_{xE} is the elastic stress, w_{oc} is the column-type initial imperfections of the stiffener, z_c is the distance from the elastic neutral axis to the outermost fiber on the compressed side, r_e is the effective radius of gyration of the cross-section of the element, I_e is the effective moment of inertia, A_s is the cross-sectional area of the element, z_0 is the neutral axis of the element, b_e is the effective width of the attached plating, h_w is the stiffener web height, t_w is the stiffener web thickness, b_f is the stiffener flange width, t_f is the stiffener flange thickness, and σ_{ys} is the yield stress of the stiffener without an attached plate. These parameters are given by

$$\sigma_{\mathrm{yeq}} = \frac{bt\sigma_{\mathrm{yp}} + (h_w t_w + b_f t_f)\sigma_{\mathrm{ys}}}{bt + h_w t_w + b_f t_f}$$

$$\lambda_e = \sqrt{\frac{\sigma_{\mathrm{yeq}}}{\sigma_{\mathrm{xE}}}}$$

$$\sigma_{\mathrm{xE}} = \frac{\pi^2 E I_e}{a^2 A_s}$$

$$\eta = \frac{w_{oc} z_c}{r_e^2}$$

$$r_e = \sqrt{\frac{I_e}{A_s}}$$

$$A_s = bt + h_w t_w + b_f t_f$$

$$z_0 = \frac{0.5 b_e t^2 + h_w t_w \left(t + 0.5 h_w\right) + b_f t_f (t + h_w + 0.5 t_f)}{b_e t + h_w t_w + b_f t_f}$$

$$I_e = \frac{b_e t^3}{12} + b_e t \left(z_0 - \frac{t}{2}\right)^2 + \frac{h_w^3 t_w}{12} + h_w t_w \left(z_0 - t - \frac{h_w}{2}\right)^2 + \frac{b_f t_f^3}{12} + b_f t_f \left(t + h_w + \frac{t_f}{2} - z_0\right)^2$$

2.3 Checking criteria of UBMs

The UBMs of a vessel at any given cross-section are evaluated using the following Equation (9) (IACS, 2024).

$$M_u \geqslant \gamma_R M \tag{9}$$

where:

$$\gamma_R = \gamma_M \gamma_{\mathrm{DB}}$$
$$M = \gamma_S M_{\mathrm{sw}} + \gamma_w f_\beta M_{\mathrm{wv}}$$

γ_M is the partial safety factor for the vertical hull girder's ultimate bending capacity, encompassing uncertainties in material, geometric, and strength prediction, γ_M = 1.1; γ_{DB} is the partial safety factor for the vertical hull girder's ultimate bending capacity, encompassing the double bottom bending effects, with γ_{DB} = 1.10 for hogging, and γ_{DB} = 1.0 for sagging; γ_S is the partial safety factor for the still water bending moment, γ_S = 1.0; γ_w is the partial safety factor for the vertical wave bending moment, γ_w = 1.2; f_β is the heading correction factor, f_β = 1.05; M is the vertical bending moment; M_{sw} is the permissible still water bending moment determined as follows.

Hogging conditions:

$$M_{\mathrm{sw-h}} = f_{\mathrm{sw}} \left(171 C_w L^2 B \left(C_B + 0.7\right) 10^{-3} - M_{\mathrm{wv-h}}\right)$$

Sagging conditions:

$$M_{\mathrm{sw-s}} = -0.85 f_{\mathrm{sw}} \left(171 C_w L^2 B \left(C_B + 0.7\right) 10^{-3} + M_{\mathrm{wv-s}}\right)$$

M_{wv} is the vertical wave bending moment.

Hogging conditions:

$$M_{\mathrm{wv-h}} = 0.19 f_{\mathrm{nl-vh}} f_m f_p C_w L^2 B C_B$$

Sagging conditions:

$$M_{\mathrm{wv-s}} = -0.19 f_{\mathrm{nl-vs}} f_m f_p C_w L^2 B C_B$$

3 Damage factors and selected vessel

3.1 Pitting corrosion

Corrosion in ship structures may arise from various causes, such as friction, chemical reactions, cavitation, operational conditions, structural design flaws, and fabrication processes. Common types of corrosion observed in marine structures include general, pitting, differential aeration, galvanic, stress, and non-uniform corrosion. The specific type and location of corrosion in ship structures are determined by their underlying causes and affected areas. Among these, pitting corrosion is the most prevalent, appearing early and frequently in ship hulls, particularly in cargo holds, ballast tanks, and fuel tanks (Vu and Dong, 2020).

Key characteristics of pitting corrosion include pit depth, pit width, pit shape, the DOP, DOC, and ΔV. Numerous studies have evaluated the impact of these characteristics on plate structures, plate-stiffener combinations, and entire ship hulls. In these analyses, the DOP is typically assumed to be 5%, 10%, 20%, 30%, and 40%, and the DOC is modeled at 10%, 20%, and 40%. The combination of the DOP and DOC defines ΔV according to Equation (10) (Momčilović et al., 2023), with values between 0.5% to 16%, and is usually considered discontinuous (Piscopo and Scamardella, 2021).

$$\Delta V = \mathrm{DOP} \cdot \mathrm{DOC} \tag{10}$$

Two primary approaches exist for representing pitting corrosion in structural parts. The first involves numerical simulation, in which pitting corrosion is represented as discrete pits on the plate surface with various shapes, such as spherical, cylindrical, or conical, and characterized by different parameters, including diameter, depth, and DOP (Feng et al., 2020; Zhang et al., 2017a, 2017b). The second approach entails 3D scanning the surface of the corroded plating and reconstructing it for subsequent analysis (Zima et al., 2025). In this study, a theoretical method is adopted rather than a numerical simulation approach, which does not allow for modeling individual corrosion pits within the structure. Therefore, a practical solution is required to integrate the effect of localized pitting corrosion into the ship hull structure. To address this, the concept of equivalent thickness is employed to determine the thickness of the corroded plate (Figure 2) (Woloszyk and Garbatov, 2023).

If pitting corrosion develops in the structures of ships, the thickness of the structural components will be less than the original value for attached plating, web plates, and flange plates. If these conditions are met, the equivalent thickness (t_{eq}) is used to assess the effective thickness of corroded structural elements, according to Equation (11) (Momčilović et al., 2023).

$$t_{eq} = t(1 - \Delta V) \tag{11}$$

where t is the original thickness of the attached plating.

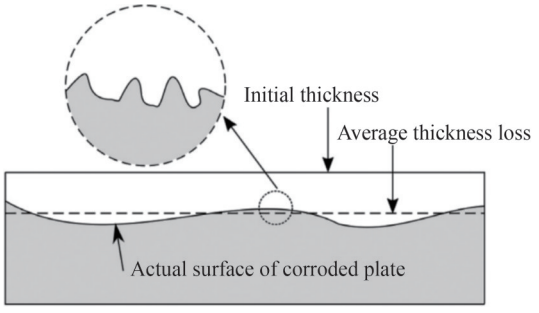


Figure 2 Concept of equivalent thickness due to pitting corrosion (Woloszyk and Garbatov, 2023)

Pitting damage can appear in any area of a ship hull with different DOP and DOC values. Over time, both the DOP and DOC increase, leading to a gradual increase in ΔV. Therefore, in this study, ΔV is assumed to incrementally increase from 0% to 30% to assess the impact of pitting damage on the HGUS of double-hull OTs. The analysis further assumes that pitting damage is uniformly distributed across all structural elements of the hull.

3.2 Initial imperfections

Initial imperfections usually appear after the ship is constructed, caused by undesirable welding and assembly operations. The six common types of initial imperfections are as follows:

Initial imperfection of the plating between the stiffeners,

$$w_{opl} = A_0 \sin\frac{m\pi x}{a}\sin\frac{\pi y}{b}$$

$$w_{oc} = B_0 \sin\frac{\pi x}{a}\sin\frac{\pi y}{B}$$

Sideways initial imperfection of the stiffener,

$$w_{os} = C_0\frac{z}{h_w}\sin\frac{\pi x}{a}$$

Residual stress in the plating between the stiffeners, σ_{rc}^{p} (compressive) or σ_{rt}^{p} (tensile).

Residual stress in the stiffener web, σ_{rc}^{s} (compressive) or σ_{rt}^{s} (tensile), and Softening in the heat-affected zone.

A_0 is the maximum magnitude of initial imperfection, as specified in Table 1; B_0 and C_0 are shown in Figure 3 and are assigned a value of $0.001a$; σ_{rtx} is tensile stress, with $\sigma_{rtx} = \sigma_y$.

These six types of initial damage are classified into two groups: initial imperfections and residual stresses (ISSC, 2012).

The imperfections during the ship construction are structural irregularities caused by cutting, forming, bending, assembly, and welding processes. These imperfections typically occur in plating between stiffeners, slide-way misalignments of stiffeners, and column-like imperfections of stiffeners, as illustrated in Figure 3 (ISSC, 2012).

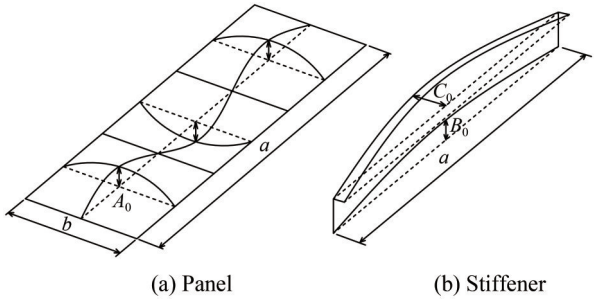


Figure 3 Initial imperfections (ISSC, 2012)

Residual stresses are generally due to the welding used to join the stiffeners to the plating. This relief fails, and subsequent molding through the gating of the stiffeners leads to stresses in the plating that surround the weld lines of the stiffeners during plating. As shown in Figure 4, the distribution of the residual stress is a compressive zone and tensile zone on both sides of the weld line (ISSC, 2012).

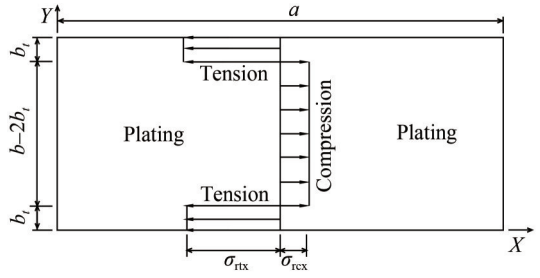


Figure 4 Residual stresses (ISSC, 2012)

The maximum levels of initial imperfections of the structural components are summarized in Table 1.

Table 1 Initial imperfection levels (ISSC, 2012)

Levels	A_0 (mm)	σ_{rcx} (MPa)
Slight	$0.025\beta^2 t$	$-0.05\sigma_y$
Average	$0.1\beta^2 t$	$-0.15\sigma_y$
Severe	$0.3\beta^2 t$	$-0.3\sigma_y$

3.3 Vessel application

To investigate the resonance effects of the aforementioned damage factors on ship hull strength, a double-hull OT was selected as the case study. This vessel has principal dimensions of 315 m in length between perpendiculars, 58 m in breadth, 30.3 m in depth, and a deadweight

capacity of 313 000 t. The vessel features a double bottom, double side, and longitudinal bulkhead structural configuration. The materials utilized include regular and high-strength steel, with yield stresses of 313.6 MPa for the steel plates and 313.6 MPa and 352.8 MPa for the longitudinal members. Figure 5 depicts the midship cross-sectional structure, providing detailed material yield strengths (ISSC, 2012).

In Figure 5, the numbers 1 through 47 represent the classification of stiffeners, the dimensions of which are provided in Table 2.

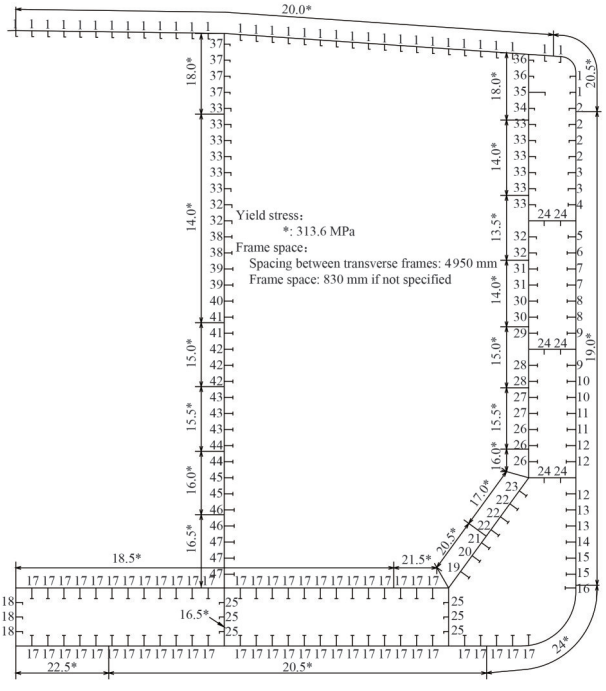


Figure 5 Midship scantlings (ISSC, 2012)

3.4 Modifications of the method

To evaluate the behavior of aged ship structures, the potential damage must be assumed and included in the structure. Equations (4) and (5), which determine the UBMs, and Equations (6)–(8), which calculate the ultimate stress of the structure, were developed, neglecting the initial imperfections and pitting damage. Therefore, it is necessary to modify these equations to incorporate these damages for each structural element. The following sections

Table 2 Longitudinal stiffeners' dimensions (ISSC, 2012)

No.	Dimensions (mm)	Type	σ_y (MPa)	No.	Dimensions (mm)	Type	σ_y (MPa)
1	300 × 90 × 13/17	AB	313.6	25	250 × 90 × 12/16	AB	313.6
2	350 × 100 × 12/17	AB	313.6	26	450 × 11 + 150 × 22	T	352.8
3	400 × 100 × 11.5/17	AB	313.6	27	450 × 11 + 150 × 19	T	352.8
4	400 × 11 + 150 × 12	T	313.6	28	450 × 11 + 150 × 16	T	352.8
5	400 × 11 + 150 × 14	T	313.6	29	450 × 11 + 150 × 14	T	352.8
6	450 × 11 + 150 × 12	T	313.6	30	450 × 11 + 150 × 12	T	352.8
7	450 × 11 + 150 × 14	T	313.6	31	450 × 11 + 150 × 14	T	352.8
8	450 × 11 + 150 × 16	T	313.6	32	400 × 100 × 11.5/16	AB	352.8
9	450 × 11 + 150 × 19	T	313.6	33	350 × 100 × 12/17	AB	352.8
10	450 × 11 + 150 × 22	T	313.6	34	300 × 90 × 13/17	AB	352.8
11	450 × 11 + 150 × 25	T	313.6	35	850 × 17 + 150 × 19	L	352.8
12	500 × 11 + 150 × 28	T	313.6	36	250 × 90 × 12/16	AB	352.8
13	500 × 11 + 150 × 30	T	313.6	37	300 × 90 × 12/16	AB	352.8
14	500 × 11 + 150 × 32	T	313.6	38	400 × 11 + 150 × 14	T	352.8
15	500 × 11 + 150 × 34	T	313.6	39	450 × 11 + 150 × 12	T	352.8
16	550 × 12 + 150 × 30	T	313.6	40	450 × 11 + 150 × 14	T	352.8
17	550 × 12 + 150 × 25	T	313.6	41	450 × 11 + 150 × 16	T	352.8
18	350 × 100/12/17	AB	313.6	42	450 × 11 + 150 × 19	T	352.8
19	550 × 12.5 + 150 × 32	T	352.8	43	450 × 11 + 150 × 22	T	352.8
20	500 × 11.5 + 150 × 30	T	352.8	44	450 × 11 + 150 × 25	T	352.8
21	500 × 11.5 + 150 × 28	T	352.8	45	450 × 11 + 150 × 28	T	352.8
22	500 × 11 + 150 × 25	T	352.8	46	500 × 11 + 150 × 25	T	352.8
23	450 × 11 + 150 × 28	T	352.8	47	500 × 11 + 150 × 28	T	352.8
24	250 × 12.5	FB	313.6				

will discuss techniques to solve the above issue.

Initial imperfections distort attached plating and plating between stiffeners, which may result in dimensions larger or smaller than the original. Therefore, considering the influence of initial imperfections, the effective width (b_e) of the attached plate is used for the initial attached width, as follows (Vhanmane and Bhattacharya, 2008):

Equation (12) is used to determine the attached width as classified in subsection 2.2, as follows:

$$\frac{b_e}{b} = \frac{\sigma_{\text{xav}} + \sigma_{\text{rx}}}{\sigma_{\text{xmax}}} \tag{12}$$

where σ_{rx} denotes the welding-induced residual stress inside the plating, σ_{xmax} denotes the maximum value of axial compressive stresses, and σ_{xav} denotes the mean axial compressive stress value.

The σ_{xmax} is determined at $y = b_t$ or $y = b - b_t$ (Figure 4), as follows (Hughes and Paik, 2010):

$$\sigma_{\text{xmax}} = \sigma_{\text{xav}} + \sigma_{\text{rtx}} - \frac{Em^2\pi^2}{8a^2} A\left(A + 2A_0\right)\cos\left(\frac{2\pi b_t}{b}\right) \tag{13}$$

The breadth of the tensile residual stress zone (Figure 4), b_t, is obtained by equilibrium condition, as follows (Hughes and Paik, 2010):

$$\frac{2b_t}{b} = \frac{\sigma_{\text{rcx}}}{\sigma_{\text{rcx}} - \sigma_{\text{rtx}}} \tag{14}$$

where A is the unknown amplitude of the added imperfection, and m is the buckling mode half-wave number in the x direction.

Conversely, according to the assumptions, pitting corrosion decreases the thickness of the entire structural elements in the affected regions. Therefore, to incorporate the effects of corrosion, the thicknesses of the attached plate (t_p), stiffener web (t_w), and stiffener flange (t_f) are modified. Equation (11) is thus rewritten as follows:

$$t_p = t_{p_\text{ini}}(1 - \Delta V) \tag{15a}$$

$$t_w = t_{w_\text{ini}}(1 - \Delta V) \tag{15b}$$

$$t_f = t_{f_\text{ini}}(1 - \Delta V) \tag{15c}$$

where t_{p_ini} denotes the plate's original thickness, t_{w_ini} represents the stiffener web's initial thickness, and t_{f_ini} represents the stiffener flange's initial thickness.

In Equations (3)−(8), the parameters including the initial attached width (b), attached plate thickness (t_p), web plate thickness (t_w), and flange plate thickness (t_f), are substituted by the effective width (b_e), calculated according to Equation (12), and the equivalent thickness, defined by Equation (15).

4 Results

For intact structures, UHBM and USBM are obtained using Equations (4) and (5). These parameters are compared with the results in the ISSC (2012) report, as presented in Table 3.

Table 3 Validations of the results (ISSC, 2012)

Method	M_{uh} (MN·m)	Dev. (%)	M_{us} (MN·m)	Dev. (%)
Current study	29066		27504	
ABAQUS (CR)	31006	6.7	24995	9.1
ANSYS (ISR)	30106	3.6	28175	2.4
CSR (CR)	29847	2.7	25014	9.1

Table 3 shows that the largest deviation of UHBM is ⩽6.7%, whereas the value of USBM is ⩽9.1%. This proves that the method applied in the paper achieved suitable and reliable results.

4.1 Case of initial imperfections

The hull is inevitably affected by initial imperfections. This effect is illustrated in Figure 6, where the UBMs are reduced to varying degrees depending on the magnitude of the imperfections. For minor defects, the UBMs are almost untouched, resulting in a small reduction of approximately 0.03% concerning the healthy structure. However, the greater the severity of any imperfections, the more pronounced the reduction in UBMs: ~1.18% at the average level of damage. The biggest reductions are noted under severe imperfections, when the UBMs are reduced by 8.48% in hogging and 7.88% in sagging. These results highlight the extent to which extreme imperfections can severely compromise the hull strength.

Figure 6 shows that the values of UBMs are all greater than the values of the required bending moments for all cases of damage levels on the structure. This concludes that the initial imperfections do not reduce the strength of the ship below the allowable level. The ship's structure is still guaranteed to be durable and reliable in operation.

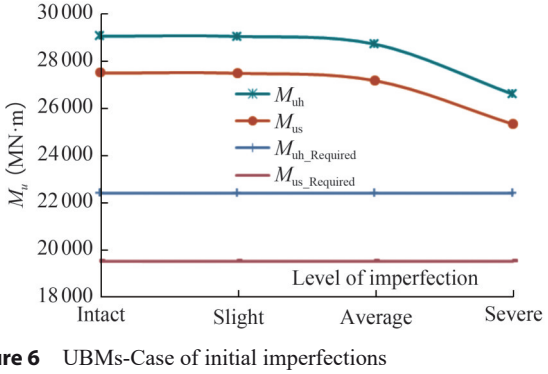


Figure 6 UBMs-Case of initial imperfections

4.2 Case of pitting corrosion

In the case of pitting corrosion, the UBMs under both hogging and sagging conditions are significantly reduced. The reduction in UBMs is proportional to the increase in ΔV. Specifically, when ΔV reaches 30%, UBMs decrease by approximately 23%, compared to the intact structure case (Figure 7). A notable point in the results shown in Figure 7 is that the failure point of the UHBM is earlier than that of USBM. More specifically, UHBM equals the required bending moment when ΔV = 19.9%, whereas USBM equals the required bending moment when ΔV = 24.7%. This suggests that pitting corrosion presents a more significant threat to the hull's ultimate strength, especially when the ship is at a wave peak.

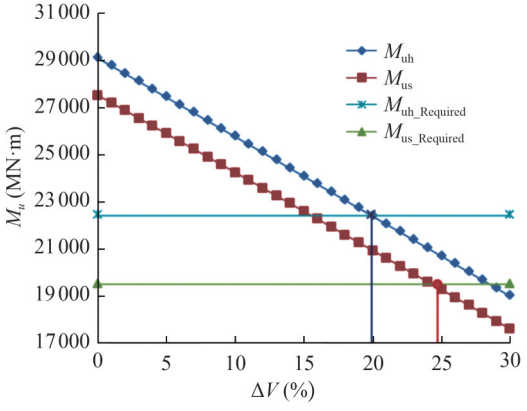


Figure 7 UBMs-Case of pitting corrosion

Pitting corrosion has a more pronounced impact on the ultimate hull strength than initial imperfections. The maximum initial imperfection level only reduces the UHBM by approximately 8.5%, while a ΔV of about 7.4% due to corrosion results in a comparable reduction. At ΔV = 30%, the UBMs decrease by more than three times compared to the structure with the highest level of initial imperfections.

4.3 Case of pitting corrosion and initial imperfections

In practice, ship hull structures are typically subject to multiple damage types simultaneously. This study specifically examines the synergistic effects of initial imperfections and pitting corrosion on the residual capacity of double-hull oil carriers. The following sections present the UBM degradation results under two wave conditions.

Figure 8 illustrates the relationship between UHBM and ΔV, showing that the presence of pitting damage and initial imperfections causes a gradual decreasing trend in the curves, observed for a combination of pitting damage with slight or moderate initial imperfections. Meanwhile, for the M_{uh}–ΔV curve in the case of pitting damage combined with severe initial imperfections, UHBM decreases steadily as ΔV increases from 0% to 23%, but exhibits a slight increase when ΔV increases from 23% to 30%. The fluctuation of UHBM indicates the pronounced impact of severe initial defects on the structure's response.

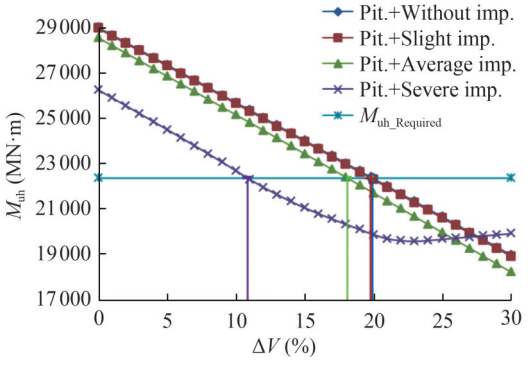


Figure 8 UHBM-Case of pitting corrosion and initial imperfections

The maximum deviations of UHBM and the points at which the required UBM is met are summarized in Table 4. Accordingly, the largest reduction in UHBM, approximately 37.17%, occurs for the structure with pitting corrosion (ΔV = 30%) combined with average initial imperfections. When the structure contains pitting damage and severe initial imperfections, UHBM decreases by 31.33% at ΔV = 23% relative to its initial value. Table 4 presents the unsatisfactory points of UHBMs. Specifically, UHBM first meets the required UBM at ΔV = 10.84% for the case of severe initial imperfections and latest when ΔV = 19.92% for the case of the structure with single pitting damage.

Table 4 Deviations of UHBM

Level of imperfections	Intact	Slight	Average	Severe
Maximum deviations of UHBM (%)	34.59	34.77	37.17	31.33
UHBMs meet the requirement at ΔV (%)	19.92	19.79	18.10	10.84

Similarly, the results for USBM are illustrated and presented in Figure 9 and Table 5, respectively. The variation trends of USBM are similar to UHBM fluctuations, but the reduction rate is larger. Specifically, the largest reduction of USBM is 38.5% (Table 5), compared to the value of 37.17% of UHBM (Table 4). The results in Table 5 indicate that USBM reaches the required value of UBM more slowly than UHBM. Specifically, USBM equals the required UBM when ΔV changes from 16.38% to 24.29% depending on the damage cases.

It is interesting to note that the curves of UHBM vs ΔV (Figure 8) and USBM vs ΔV (Figure 9) for the case of pitting corrosion and severe initial imperfections recover when ΔV is greater than 22%. This is because when the initial imperfections are severe, the effective attached width (b_e) increases and can be larger than the initial one (b), particularly in structural elements belonging to the inner side and longitudinal bulkheads. Consequently, UHBM and USBM will increase accordingly.

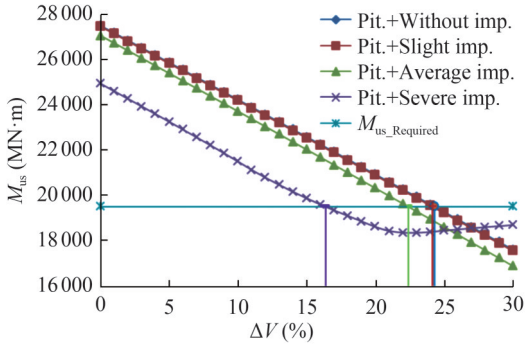


Figure 9 USBM-Case of pitting corrosion and initial imperfections

Table 5 Deviations of USBM

Level of imperfections	Intact	Slight	Average	Severe
Maximum deviations of USBM (%)	35.90	36.07	38.50	31.95
USBMs meet the requirement at ΔV (%)	24.29	24.16	22.39	16.38

4.4 Safety factors of UBMs

UBM safety factor is used as a significant index for evaluating the residual strength of ship hull structures. Higher residual strength corresponds to increased vessel reliability, and an operational factor of 1.0 means that UBMs are equal to the regulatory bending moments from the regulations, with any further increase potentially causing structural failure. Tables 5 and 7 show the safety factors for the structures subjected only to initial imperfections and the combined effects of pitting corrosion and initial imperfections, respectively.

For imperfect structures, the safety factor decreases with increased imperfection severity, from 1.30 to 1.19 in the hogging condition and 1.41 to 1.30 in the sagging condition. As summarized in Table 6, in the case of the most extreme level of initial imperfections, the safety factor is still approximately 1.2, which suggests that the ship hull has enough residual strength to satisfy the need for use.

In critical scenarios, when preparing for unreliable structures including both pitting corrosion and initial imperfection, the safety factor for UBMs is significantly reduced and even falls below 1.0 in certain situations, as indicated in Table 7. Grounded by deviations, at average-level initial imperfections, the safety factor decreases to 0.81 when ΔV = 30% of the threshold (ΔV) values at which the safety factor = 1.0 for eight damage scenarios are further delineated in Table 7. The key ΔV values vary between 10.84% and 24.29%, depending on the combination of pitting corrosion and initial imperfections.

Table 6 Safety factors for the case of initial imperfections

Ratios	Levels of imperfection			
	Intact	Slight	Average	Severe
M_{uh}/M_{uh-req}	1.30	1.30	1.28	1.19
M_{us}/M_{us-req}	1.41	1.41	1.39	1.30

5 Discussions

The results obtained in this study elucidate the pronounced influences that pitting corrosion and initial imperfections have on the RUBS of double-hull OTs. Besides, this study contributes to the structural mechanics understanding of the aging ship hull and leads to considerable guidance for their maintenance strategies and safety management in the marine field.

The effects of initial imperfections on RUBS are aggravated by the early pitting corrosion discussed in our study. Although individual micro-initial defects have a negligible effect in slight conditions, the combination of the micro-initial defects and pitting corrosion can considerably decrease RUBS, particularly in hogging and sagging moments. This result highlights the importance of consideration for threshold damage factors in the structural assessment of ships for their safety and reliability.

The research identifies cross-over points after which RUBS fails to meet design specifications. For instance, under simple pitting conditions, RUBS could not satisfy the needed moment of bending when the corrosion ΔV reached

Table 7 Safety factors of UBMs

Ratios	Cases of pitting corrosion and varying levels of initial imperfections	Max. Ratios (at ΔV = 0%)	Min. Ratios (at ΔV = 30%)	ΔV when ratios = 1
M_{uh}/M_{uh_rep}	Intact	1.30	0.85	ΔV = 19.9%
	Slight	1.30	0.85	ΔV = 19.79%
	Average	1.28	0.81	ΔV = 18.10%
	Severe	1.17	0.89	ΔV = 10.84%
M_{us}/M_{us_req}	Intact	1.41	0.90	ΔV = 24.29%
	Slight	1.41	0.90	ΔV = 24.16%
	Average	1.39	0.87	ΔV = 22.39%
	Severe	1.28	0.96	ΔV = 16.38%

19.9%. This threshold drops markedly, to ΔV = 10.84%, when this is paired with extreme initial imperfections. These threshold values are necessary indicators to trigger the maintenance and inspections, providing practical value for the ship operators and engineers.

This study calculated safety factors, and the results show that RUBS experiences severe degradation during combined damage scenarios. Here, for instance, with average initial imperfections, the safety factor drops to 0.81, which is under a threshold of 1.0 at ΔV = 30%, indicating structural failure. The present results also underscore the immediate need for enhanced maintenance tactics and tracking systems for operational safety.

Future studies should extend the range of this study to include other ship types, including BCs and container vessels, and investigate the influence of environmental aspects, such as variable ambient conditions and seawater chemistry, and dynamic loading, such as wave-induced loading. Model reliability can be continuously improved through experimental validation via lab testing and field operational data. Predictive tools using machine learning are also important for real-time damage assessment and estimating the remaining useful life of the structure. Alleviating such damage, through innovative protective solutions such as improved coatings, structural reinforcements, and new maintenance protocols, is another area of research focus, to increase the resilience of ship hulls

6 Conclusions

This study proposed a method for determining UBMs by incorporating the effects of initial imperfections and pitting corrosion. An OT was used as a case study to evaluate the resonance effects of these damage factors. The UBMs and their corresponding safety factors were calculated, analyzed, and discussed, yielding the following key findings:

First, the effect of initial imperfections on UBMs was minimal under most conditions, with significant reductions observed only at the highest severity level, resulting in an 8.5% decrease in UBMs.

Second, pitting corrosion led to a gradual decline in UBMs. When ΔV reached 30%, UHBM decreased by 23.0%, while USBM decreased by 23.8%, indicating that USBM is more sensitive to pitting corrosion.

Third, the combined effect of pitting corrosion and initial imperfections resulted in greater substantial reductions in UBMs than the impact of either factor alone. The most significant decrease occurred at ΔV = 30%, with an average level of initial imperfections, where UHBM was reduced by 37.17% and USBM by 38.50%.

Fourth, the critical thresholds for UBMs differed depending on the damage scenario. For UHBM, the required bending moment was achieved at ΔV = 19.9% for pitting corrosion alone and ΔV = 10.84% when combined with severe initial imperfections, whereas for USBM, these thresholds occurred at ΔV = 24.7% and ΔV = 16.38%, respectively.

Finally, the safety factors for UBMs decreased significantly under combined damage scenarios, as detailed in Tables 6 and 7. These reductions underscore the importance of careful monitoring and maintenance to ensure the structural integrity and operational safety of the hull.

These findings emphasize the critical importance of evaluating the combined effects of multiple damage factors, offering valuable insights for researchers and ship owners to enhance structural resilience and safety during OT operations.

Competing interests Van Tuyen Vu is an editorial board member for the Journal of Marine Science and Application and was not involved in the editorial review, or the decision to publish this article. All authors declare that there are no other competing interests.

References

Ahmadi F, Ranji AR (2024) Reliability assessment of ship hull girders considering pitting corrosion and crack. Engineering Research Express 6(1): 1-13. https://doi.org/10.1088/2631-8695/ad2641

Cui JJ, Wang DY, Ma N (2017) A study of container ship structures' ultimate strength under corrosion effects. Ocean Engineering 130: 454-470. https://doi.org/10.1016/j.oceaneng.2016.11.061

Cui JJ, Wang DY, Ma N (2018) Case studies on the probabilistic characteristics of ultimate strength of stiffened panels with uniform and non-uniform localized corrosion subjected to uniaxial and biaxial thrust. International Journal of Naval Architecture and Ocean Engineering 11(1): 97-118. https://doi.org/10.1016/j.ijnaoe.2018.02.011

Faqih I, Adiputra R, Prabowo AR, Muhayat N, Ehlers S, Braun M (2023) Hull girder ultimate strength of bulk carrier (HGUS-BC) evaluation: Structural performances subjected to true inclination conditions of stiffened panel members. Results in Engineering 18: 101076. https://doi.org/10.1016/j.rineng.2023.101076

Feng L, Hu L, Chen XG, Shi H (2020) A parametric study on effects of pitting corrosion on stiffened panels' ultimate strength. International Journal of Naval Architecture and Ocean Engineering 12(2020): 699-710. https://doi.org/10.1016/j.ijnaoe.2020.08.001

Guedes Soares C, Garbatov Y (1996) Reliability of maintained ship hulls subjected to corrosion. Journal of Ship Research 40(3): 235-243. https://doi.org/10.5957/jsr.1996.40.3.235

Guedes Soares C, Garbatov Y (1999) Reliability of maintained ship hulls subjected to corrosion and fatigue under combined loading. Journal of Constructional Steel Research 52(1): 93-115. https://doi.org/10.1016/S0143-974X(99)00016-4

Hughes OF, Paik JK (2010) Ship structural analysis and design. The Society of Naval Architects and Marine Engineers, Alexandria, USA

IACS (2024) Common structural rules for bulk carriers and oil tankers. Available from https://iacs. org. uk/resolutions/common-structural-rules/csr-for-bulk-carriers-and-oil-tankers [Accessed on Jan. 01, 2025]

ISSC (2012) Committee III. 1 Ultimate strength. The 18th International

Ship and Offshore Structures Congress, Rostock, Germany. https://www.academia.edu/18936028/ISSC12_18th_International_Ship_and_Offshore_Structure_Congress

Kakaie A, Garbatov Y, Guedes Soares C (2026) Time-dependent ship hull reliability accounting for non-stationary stochastic degradation process. Reliability Engineering & System Safety 265: 111602. https://doi.org/10.1016/j.ress.2025.111602

Kim DK, Liew MS, Youssef SAM, Mohd MH, Kim HB, Paik JK (2014) Time-dependent ultimate strength performance of corroded FPSOs. Arabian Journal for Science and Engineering 39(11): 7673-7690. https://doi.org/10.1007/s13369-014-1364-4

Liu B, Garbatov Y, Zhu L, Guedes Soares C (2018) Numerical assessment of the structural crashworthiness of corroded ship hulls in stranding. Ocean Engineering 170: 276-285. https://doi.org/10.1016/j.oceaneng.2018.10.034

Momčilović N, Ilić N, Kalajdžić M, Ivošević S, Petrović A (2023) Pitting and uniform corrosion effects on ultimate strength of a bulk carrier. Procedia Structural Integrity 48: 12-18. https://doi.org/10.1016/j.prostr.2023.07.104

Momčilović N, Ilić N, Kalajdžić M, Ivošević S, Petrović A (2024) Effect of corrosion-induced structural degradation on the ultimate strength of a high-tensile-steel ship hull. Journal of Marine Science and Engineering 12(5): 745. https://doi.org/10.3390/jmse12050745

Nouri Z, Khedmati MR (2020) Progressive collapse analysis of an FPSO vessel hull girder under vertical bending considering different corrosion models. Journal of Marine Science and Application 19(4): 674-692. https://doi.org/10.1007/s11804-020-00173-z

Paik JK, Mansour AE (1995) A simple formulation for predicting the ultimate strength of ships. Journal of Marine Science and Technology 1(1): 52-62. https://doi.org/10.1007/BF01240013

Paik JK, Thayamballi AK, Lee JM (2004) Effect of initial deflection shape on the ultimate strength behavior of welded steel plates under biaxial compressive loads. Journal of Ship Research 48(1): 45-60. https://doi.org/10.5957/jsr.2004.48.1.45

Paik JK, Wang G, Thayamballi AK, Lee JM, Park YI (2003) Time-dependent risk assessment of aging ships accounting for general pit corrosion, fatigue cracking and local dent damage. For presentation at the 2003 SNAME Annual Meeting, World Maritime Technology Conference, San Francisco, USA

Piscopo V, Scamardella A (2021) Incidence of pitting corrosion wastage on the hull girder ultimate strength. Journal of Marine Science and Application 20(3): 477-490. https://doi.org/10.1007/s11804-021-00218-x

Putranto T, Kõrgesaar M, Tabri K (2022) Application of equivalent single-layer approach for ultimate strength analyses of ship hull girder. Journal of Marine Science and Engineering 10(10): 1-20. https://doi.org/10.3390/jmse10101530

Rahbar-Ranji A, Niamir N, Zarookian A (2015) Ultimate strength of stiffened plates with pitting corrosion. International Journal of Naval Architecture and Ocean Engineering 7(3): 509-525. https://doi.org/10.1515/ijnaoe-2015-0037

Saad-Eldeen S, Garbatov Y, Guedes Soares C (2013) Ultimate strength assessment of corroded box girders. Ocean Engineering 58: 35-47. https//doi.org/10.1016/j.oceaneng.2012.09.019

Sultana S, Wang Y, Sobey AJ, Wharton JA, Shenoi RA (2015) Influence of corrosion on the ultimate compressive strength of steel plates and stiffened panels. Thin-Walled Structures 96: 95-104. https://doi.org/10.1016/j.tws.2015.08.006

Tekgoz M, Garbatov Y, Guedes Soares C (2020) Review of ultimate strength assessment of ageing and damaged ship structures. Journal of Marine Science and Application 19: 512-533. https//doi.org/10.1007/s11804-020-00179-7

Vhanmane S, Bhattacharya B (2008) Estimation of ultimate hull girder strength with initial imperfections. Ships and Offshore Structures 3(3): 149-158. https://doi.org/10.1080/17445300802204389

Vladimir N, Senjanović I, Jovanović I, Tomašević S, Jurišić P (2023) Direct strength calculation of an aged single-bottom tanker during its towing in waves. Proceedings of the Institution of Mechanical Engineers, Part M: Journal of Engineering for the Maritime Environment 238(2): 417-430. https://doi.org/10.1177/14750902231189917

Vu VT, Dong DT (2020) Hull girder ultimate strength assessment considering local corrosion. Journal of Marine Science and Application 19(4): 693-704. https://doi.org/10.1007/s11804-020-00169-9

Vu VT, Yang P (2017) Effect of corrosion on the ship hull of a double hull very large crude oil carrier. Journal of Marine Science and Application 16(3): 334-343. https://doi.org/10.1007/s11804-017-1425-7

Vu VT, Yang P, Doan VT (2018) Effect of uncertain factors on the hull girder ultimate vertical bending moment of bulk carriers. Ocean Engineering 148: 161-168. https://doi.org/10.1016/j.oceaneng. 2017.11.031

Wang F, Wang R, Ju JJ (2023) Ultimate compressive strength of H-section stub columns subject to random pitting corrosion damage. Applied Sciences 13(19): 11051. https://doi.org/10.3390/app131911051

Woloszyk K, Garbatov Y (2023) Advanced numerical modelling for predicting residual compressive strength of corroded stiffened plates. Thin-Walled Structures 183: 110380. https://doi.org/10.1016/j.tws.2022.110380

Woloszyk K, Goerlandt F, Montewka J (2024) A framework to analyse the probability of accidental hull girder failure considering advanced corrosion degradation for risk-based ship design. Reliability Engineering & System Safety 251: 110336. https://doi.org/10.1016/j.ress.2024.110336

Yamamoto N, Ikegami K (1998) A study on the degradation of coating and corrosion of ship's hull based on the probabilistic approach. Journal of Offshore Mechanics and Arctic Engineering 120(3): 121-128. https://doi.org/10.1115/1.2829532

Zhang J, Shi XH, Guedes Soares C (2017a) Experimental analysis of residual ultimate strength of stiffened panels with pitting corrosion under compression. Engineering Structures 152: 70-86. https://doi.org/10.1016/j.engstruct.2017.08.069

Zhang Y, Huang Y, Meng FL (2017b) Ultimate strength of hull structural stiffened plate with pitting corrosion damage under uniaxial compression. Marine Structures 56(2017): 117-136. https://doi.org/10.1016/j.marstruc.2017.07.006

Zhou HC, Kong XS, Wang Y, Zheng C, Pei ZY, Wu WG (2021) Dynamic response of hull girder subjected to combined underwater explosion and wave induced load. Ocean Engineering 235: 1-35. https://doi.org/10.1016/j.oceaneng.2021.109436

Zima B, Roch E, Mikulski T, Wójcik M (2025) Influence of corrosion degradation on the dynamic response of steel plates. Polish Maritime Research 32(2): 132-140. https://doi.org/10.2478/pomr-2025-0028